AIAA JOURNAL
Vol. 44, No. 3, March 2006

Spray Characteristics of Angled Liquid Injection into Subsonic Crossflows

M. Costa,* M. J. Melo,† and J. M. M. Sousa‡
Technical University of Lisbon, 1049-001 Lisbon, Portugal
and
Y. Levy§
Technion—Israel Institute of Technology, 32000 Haifa, Israel

The spray characteristics of angled liquid injection into subsonic crossflows were experimentally investigated. The experiments were conducted using water as the test liquid and included variations of the nozzle injection angle, air velocity of the crossflow, and liquid flow rate. An initial assessment of the spray characteristics performed with the aid of a visualization technique revealed that the overall jet penetration, breakup length, and atomization quality are significantly affected by the nozzle injection angle and, to a lesser extent, by the liquid-to-air momentum flux ratio. Subsequently, detailed droplet size and droplet velocities were obtained for various sprays by the use of phase Doppler anemometry. The data reveal that there is an evident longitudinal droplet velocity/diameter correlation for all droplets, with small droplets being faster than larger droplets. Furthermore, the droplet mean diameters diminish on increasing the nozzle injection angle but are affected only marginally by the liquid-to-air momentum flux ratio.

Nomenclature

D	=	nozzle internal diameter
H	=	wind-tunnel height
k	=	air turbulent kinetic energy
L	=	breakup length
Oh	=	Ohnesorge number, $\mu_{\text{liq}}/(\rho_{\text{liq}} D \sigma_{\text{liq}})^{1/2}$
q	=	liquid-to-air momentum flux ratio, $\rho_{\text{liq}} V_{\text{liq}}^2/(\rho_{\text{air}} U_{\text{air}}^2)$
Re_{air}	=	freestream Reynolds number, $\rho_{\text{air}} U_{\text{air}} D/\mu_{\text{air}}$
Re_{liq}	=	liquid jet Reynolds number, $\rho_{\text{liq}} V_{\text{liq}} D/\mu_{\text{liq}}$
S	=	curvilinear distance along the spray centerline from the breakup location to the measuring location
T_b	=	breakup regime parameter
U	=	droplet velocity in x direction
U_{air}	=	air velocity of the crossflow
u	=	velocity in x direction
u_{rel}	=	relative air velocity, $(U_{\text{air}} - u_{\text{liq}})/U_{\text{air}}$
V	=	droplet velocity in y direction
V_{liq}	=	liquid-injection velocity
W	=	wind-tunnel width
We_{liq}	=	liquid Weber number, $\rho_{\text{liq}} D V_{\text{liq}}^2/\sigma_{\text{liq}}$
$We_{\text{rel-air}}$	=	relative air Weber number, $\rho_{\text{air}} D(U_{\text{air}} - u_{\text{liq}})^2/\sigma$
x, y, z	=	coordinates
α	=	liquid-injection angle
μ	=	dynamic viscosity
ρ	=	density
σ	=	liquid surface tension

Subscripts

air	=	air property
b	=	at column breakup location
liq	=	jet-exit liquid property

Received 14 May 2004; accepted for publication 26 September 2005.

*Assistant Professor, Mechanical Engineering Department, Instituto Superior Técnico, Avenida Rovisco Pais; mcosta@navier.ist.utl.pt.

†Graduate Student, Mechanical Engineering Department, Instituto Superior Técnico, Avenida Rovisco Pais.

‡Assistant Professor, Mechanical Engineering Department, Instituto Superior Técnico, Avenida Rovisco Pais. Senior Member AIAA.

§Associate Professor, Faculty of Aerospace Engineering.

Introduction

DESPITE that most of the combustion equipment manufacturers already offer low-NO_x burners, there is still a great potential for pollutants reduction through design improvements. Few years ago, a special form of combustion regime called *flameless oxidation* has been presented as a means of reducing thermal NO formation.[1] Apparently, the concept can be applied to a wide range of combustion equipment including gas turbines and jet engines. The present work is part of a project whose objective is to develop a flameless oxidation combustor based on the principle of liquid fuel injection in vitiated air, which is highly diluted by internally recirculated hot flue gases.[2] To reach flameless oxidation conditions, the combustor should incorporate separate locations for the supply of liquid fuel and air into the combustion chamber. This means that the liquid fuel should be injected from the combustor walls so that the features of the liquid jet breakup and atomization in a gaseous crossflow would be of critical importance. Therefore, the purpose of the present investigation is to examine and characterize the breakup and atomization processes of a plain liquid jet in a subsonic crossflow of air.

Relevant related studies of round liquid jets in gaseous subsonic crossflows included those of Inamura and Nagai,[3] Wu et al.,[4,5] Becker and Hassa,[6] Rachner et al.,[7] Cavaliere et al.,[8] and Sallam et al.,[9] among others. These studies have examined the breakup and penetration of plain jets in subsonic crossflows, as well as the properties of the resulting sprays, but experiments were exclusively conducted under normal liquid injection into subsonic crossflows. Our combustor device,[2] however, requires angled liquid injection, which has been nearly ignored by researchers with the exception of the work of Fuller et al.[10] These authors employed pulsed shadowgraph photography to ascertain liquid column trajectories, column fracture locations, and near-field spray characteristics as a function of the liquid-injection angle in a transverse airflow. They concluded that the liquid column trajectories correlate with the liquid injection angle α and liquid-to-air momentum flux ratio q.

In the context of angled liquid injection into subsonic crossflows, little attention appears to have been devoted to the characterization of the resulting sprays through measurements of droplet sizes and velocities, for example, the study of Fuller et al.[10] does not report such important data. Against this background, it is clear that there is a need for investigations that should specifically address this topic.

This aspect has prompted, to some extent, the experimental investigation described here, the objective of which is to investigate the effects of the liquid-nozzle-injection angle, air velocity of the crossflow, and liquid flow rate on the breakup and atomization processes of liquid jets in a subsonic crossflow of air. To this end, an initial assessment of the spray characteristics was performed with the aid of a visualization technique based on video recording and using laser sheet illumination. Following a detailed characterization of the airflow in the tunnel with laser Doppler anemometry (LDA), detailed droplet size and droplet velocities were obtained for various sprays by the use of phase Doppler anemometry (PDA).

Experimental Apparatus and Procedure

Figure 1 shows schematics of the test section, including details of the nozzle geometry, and of the diagnostics used in the present work. Figure 2 presents a schematic of the flow along with the established coordinate system. The blowdown wind tunnel is made of PERSPEX. It is about 1.5 m long with a height $H = 150$ mm and a width $W = 100$ mm. The airflow is supplied by two independent fans, which allow the use of three different air velocities. The wind-tunnel contraction was designed to produce a rather uniform velocity profile and relatively low turbulence levels in the test section.[11] Distillate water from a pressurized tank was injected into the tunnel

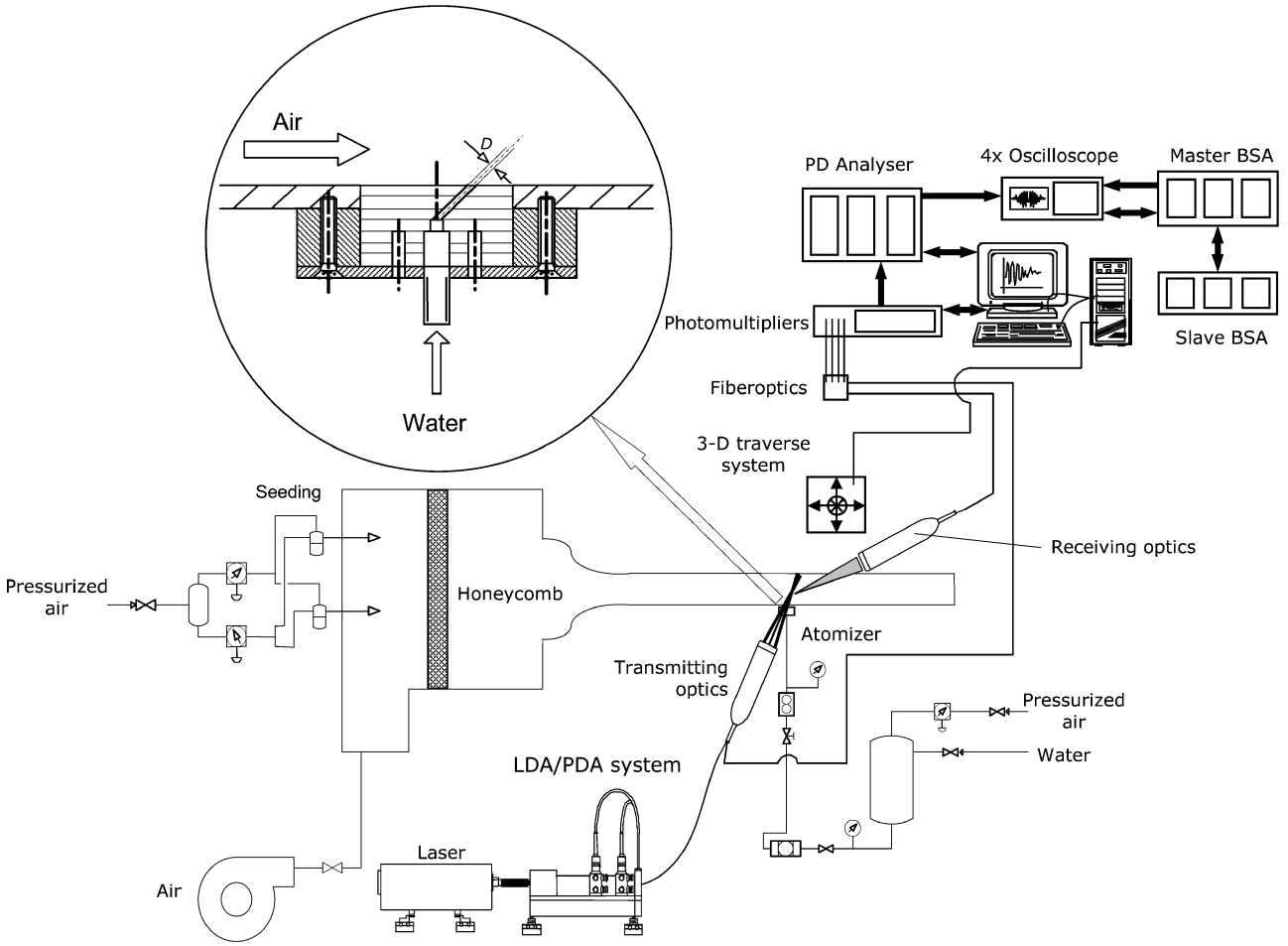

Fig. 1 Schematics of the test section, including details of the nozzle geometry and of the diagnostics.

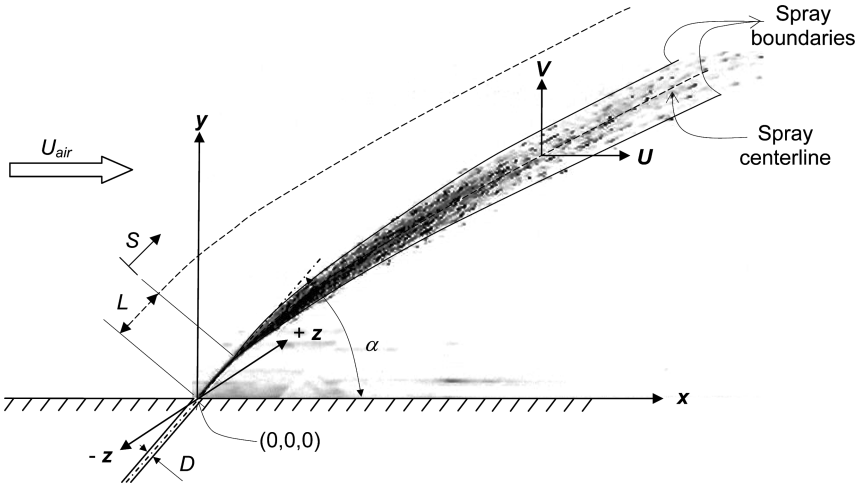

Fig. 2 Coordinate system.

through single-hole nozzles with internal diameter $D = 0.15$ mm and injection angles α of 15, 30, and 45 deg. The exit of the nozzles was sharp, and the hole length-to-diameter ratio was larger than 100 in all cases. For each nozzle, the atomization features were studied for a range of velocities of the crossflow U_{air} and of the liquid injection V_{liq}.

Before the liquid-injection experiments, the airflow in the tunnel was thoroughly characterized by the application of LDA. A two-component velocimeter from DANTEC, which was operated in the dual-beam backward-scatter mode, was employed to meet this objective, for example, see Sousa and Pereira.[12] High data rates, close to 1 kHz, were obtained by seeding the flow with small droplets of a mixture prepared with ethyleneglycol (20%) and water (80%). The droplets were generated by four medical nebulizers INSPIRON 002305-A placed at the plenum chamber of the wind tunnel, thus producing particle diameter distributions typically lying between 0.8 and 4 μm and showing a mean diameter at approximately 1 μm. Calculation of particle time constants allowed ensuring that such particles were adequately tracking the gas phase. The backscattered light collected by the receiving optics was bandpass filtered and processed by two DANTEC 57N20/57N35 Burst Spectrum Analyzers interfaced with a IBM AT compatible computer. Velocity statistics were evaluated by ensemble averaging, calculated from 10,000 samples, using BURSTware software.

The two-phase flow data reported here include instantaneous spray images obtained with the aid of a visualization technique based on video recording and using laser sheet illumination. A 5-W Ar-ion laser was employed to generate a coherent light beam 2 mm in diameter, which was expanded to a light sheet by the use of a cylindrical lens. Motion pictures were recorded at right angle to the sheet of light using a Sony SSC-M370CE video camera with a charge-coupled-device resolution of 768×576 pixels. As a result of the optical arrangements used during the experiments, the spatial resolution of video images was limited to approximately 100 μm/pixel. Aiming to digitally postprocess the acquired images, a MIRO DC-30 board interfaced with the video source was used to convert the analog video images to digital arrays. The mean values of breakup length L, spray dispersion, and stabilized angle with respect to the crossflow for a particular nozzle geometry were obtained by processing a large number of digital images. Typically, a set of 500 frames for each spray has been digitally processed using in-house MATLAB® routines.

Other quantitative data such as droplet size and droplet velocities were obtained by the use of PDA. Data collection on the centerline of the wind tunnel (liquid injection location; see Fig. 2) was based on a two-component system from DANTEC. It was operated in refraction mode for an off-axis angle close to the Brewster condition, which corresponds to 73.7 deg in the present case. This allowed taking advantage of the dominance of first-order refraction and simultaneously reducing the influence of both reflection and higher orders of refraction. The optical arrangement was such that it generated a measuring volume approximately 4 mm in length and 0.2 mm in diameter. Coupled with an effective scattering angle of 75 deg, this provided a droplet sizing range up to about 1 mm. To achieve this, the aperture plate with the smaller slits (large particles) from the set of three supplied by DANTEC was mounted in the receiving optics. The scattered light signals from four photomultipliers were processed by a DANTEC 58N10 Particle Dynamics Analyzer interfaced with the just-mentioned computer, and droplet flow statistics were calculated using SIZEware software. The signal validation procedures made use of signal-to-noise ratio, phase error, and spherical deviation criteria. The maximum errors in phase and sphericity allowed in the measurements were 20 deg and 10%, respectively. In addition, the sample size was always larger than 3000 in all measurements. However, in areas characterized by a high data rate, at least 5000 samples were used to evaluate droplet mean velocities, variance values (not shown), and diameters.

Errors incurred in the measurement of velocities by displacement and distortion of the measuring volume as a result of refraction on the tunnel walls were found to be negligibly small and within the accuracy of the measuring equipment in the case of the LDA. Regarding the PDA measurements, the SIZEware software allowed to correct the results for these effects. Nonturbulent Doppler broadening errors caused by gradients of mean velocity across the measuring volume[13] affect essentially higher-order statistics, which were not considered in the present study. The number of individual size and velocity signals employed to compute the averages led to a statistical (random) error below 1% for time-averaged values, in accordance with the analysis presented by Yanta and Smith[14] for a 95% confidence level. No efforts were made to correct the results for sampling bias. However, the systematic errors that might have arisen in this context were minimized in virtue of the high ratio between seed rates and velocity fluctuation rates, as suggested by Erdmann and Tropea.[15]

Results and Discussion

The experiments were conducted using water as the test liquid. Table 1 summarizes the operating conditions employed in the present study. Air velocities of the crossflow of 12.7, 27.3, and 43.4 m/s, liquid-injection velocities of 4.8, 7.2, 14.3, and 23.9 m/s, and liquid nozzle injection angles of 15, 30, and 45 deg were tested. The experimental range of the air velocities of the crossflow used here is significantly lower than that used by Fuller et al.[10] (from 69.2 to 138.4 m/s in their case); the present range was chosen based on numerical simulations of our combustor.[2] The resulting range of dimensionless parameters was as follows: $22.9 \le q \le 637.4$, $0.1 \le We_{\text{rel-air}} \le 3.42$, $48 \le We_{\text{liq}} \le 1190.3$, $104 \le Re_{\text{air}} \le 356$, and $726 \le Re_{\text{liq}} \le 3615$.

Figures 3 and 4 show the wind-tunnel airflow characteristics for the tested conditions. These figures present vertical profiles of the longitudinal velocity u_{air} and the turbulent kinetic energy k. It can be seen in Fig. 3 that at the lowest tested velocities the flow exhibits higher velocities close to the wall than in the channel centerline. However, this rather small departure from a typical boundary-layer profile decreases with growing values of U_{air}. The penalty for operating at significantly lower velocities than that for the wind-tunnel design condition is a larger departure from uniform flow.[11] The three-dimensional characteristics of the flow can be judged by the transverse profiles shown in Fig. 4. The observed gradients in the central plane where the liquid injection takes place are small, and therefore its influence in the liquid breakup and atomization processes is minimal.

Figure 5 shows instantaneous spray images, obtained during the visualization procedure, that illustrate the effects of liquid-injection

Table 1 Operating conditions[a] and breakup location

Test condition	α, deg	V_{liq}, m/s	Re_{liq}	We_{liq}	U_{air}, m/s	Re_{air}	$We_{\text{rel-air}}$	u_{rel}	q	x_b, mm[b]	y_b, mm[b]
1	30	4.8	726	48.0	27.3	224	1.32	0.85	25.7	13.9	8.0
2	30	7.2	1089	108.0	12.7	104	0.10	0.51	267.3	35.8	20.7
3	30	7.2	1089	108.0	27.3	224	1.10	0.77	57.8	21.7	12.5
4	30	7.2	1089	108.0	43.4	356	3.42	0.86	22.9	8.9	5.2
5	45	7.2	1089	108.0	27.3	224	1.22	0.81	57.8	7.1	7.1
6	15	7.2	1089	108.0	27.3	224	1.02	0.75	57.8	28.3	7.6
7	30	14.3	2163	426.1	27.3	224	0.55	0.55	228.2	22.3	12.9
8	30	23.9	3615	1190.3	27.3	224	0.11	0.24	637.4	26.5	15.3

[a]For all test conditions: $D = 0.15$ mm and $Oh = 0.0095$.
[b]Values of the ordinate and abscissa (referenced to the injector tip) of the breakup location.

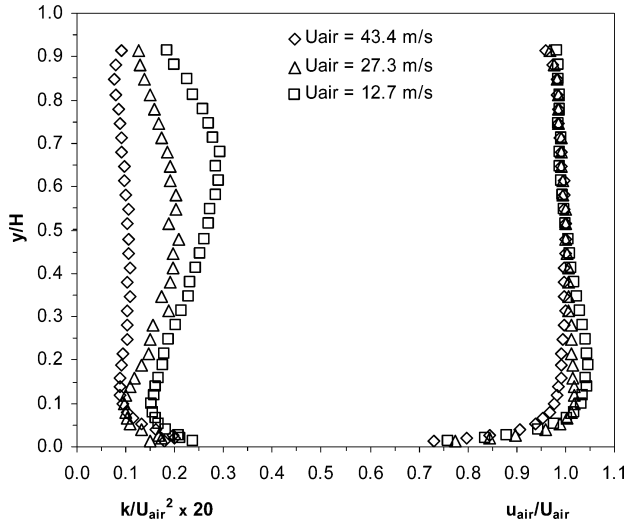

Fig. 3 Vertical velocity and turbulent kinetic energy profiles in the wind tunnel.

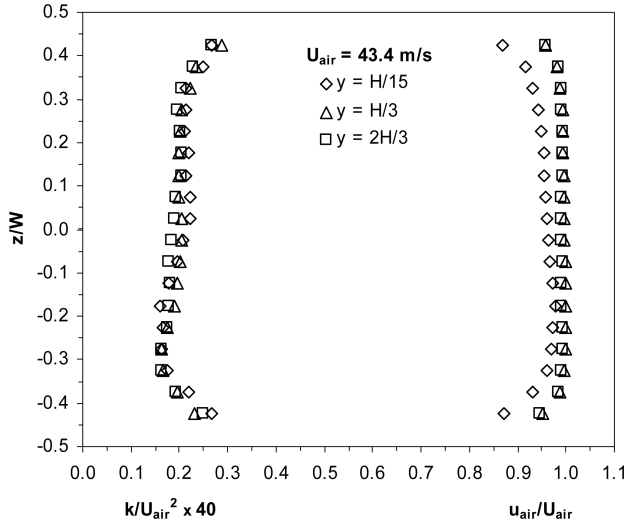

Fig. 4 Transverse velocity and turbulent kinetic energy profiles in the wind tunnel.

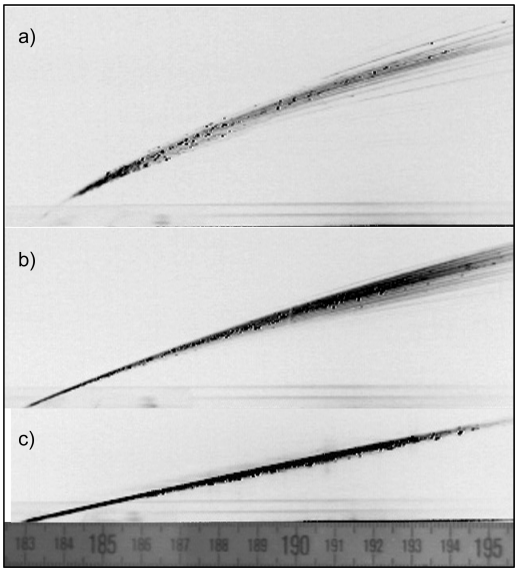

Fig. 5 Instantaneous spray images: effect of the nozzle injection angle α on the disintegration process: a) test condition 5 ($\alpha = 45$ deg and $q = 57.8$), b) test condition 3 ($\alpha = 30$ deg and $q = 57.8$), and c) test condition 6 ($\alpha = 15$ deg and $q = 57.8$).

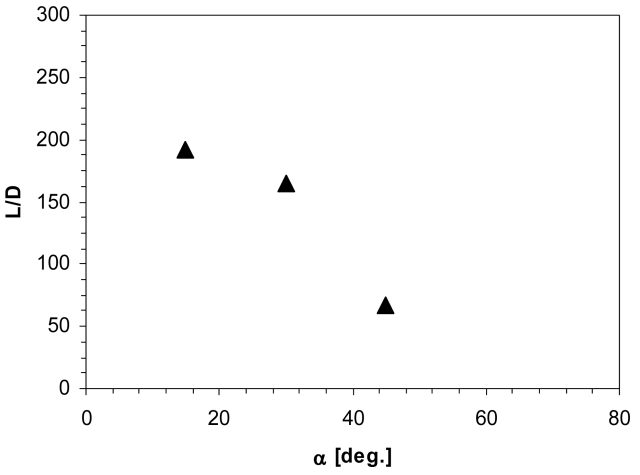

Fig. 6 Effect of the nozzle injection angle α on the breakup length (test conditions 3, 5, and 6).

angle α on the disintegration process for $V_{liq} = 7.2$ m/s, $U_{air} = 27.3$ m/s, and $q = 57.8$. Note that as the injection angle decreases, the value of u_{rel} also decreases; specifically, in this case, as α decreased from 45 to 15 deg, u_{rel} decreased from 0.81 to 0.75 (see Table 1). Consequently, a decrease in α maintaining q constant results in a reduction of the shear forces actuating on the surface of the liquid column. As can be seen in Fig. 5, as α decreases, the liquid column straightens, the overall penetration decreases within the field of view, and the atomization process deteriorates. Here, U_{air} is relatively small (27.3 m/s) so that the characteristics of nonaerodynamic column breakup (those resulting from liquid turbulence and liquid inertial forces) can be clearly identified in the lower injection angles of 15 and 30 deg. At $\alpha = 45$ deg, the enhanced effects of the aerodynamic forces are apparent as a consequence of the higher value of u_{rel}. Fuller et al.[10] used in their experiments values of U_{air} (69–138 m/s) and V_{liq} (19–54 m/s) much higher than those used in this work. In spite of this, our spray images show signs of analogous behavior to their sprays, particularly in regard to the variation of the overall jet penetration and atomization quality with the liquid-injection angle. This can be essentially attributed to the similar values of q used in both studies (57.8 in our study as compared with 48.1 in their study).

Figure 6 shows the variation of the nondimensional breakup length L (normalized by the nozzle diameter D) with the nozzle injection angle for the conditions shown in Fig. 5, that is, for a constant value of $q = 57.8$. Note that the value of the breakup length (see Fig. 2) is part of the output of the postprocessing routines developed in the course of the present work to carry out a systematic analysis of a large number of spray images. The data show that the breakup length decreases slightly with increasing nozzle injection angle from 15 to 30 deg but decreases even more with increasing nozzle injection angle from 30 to 45 deg. This is consistent with the observations from the spray images, suggesting that there is a threshold for the aerodynamic forces resulting from the presence of crossflow to effectively disintegrate the liquid column. The threshold is the Weber number, which sets the boundaries to the various breakup regimes of jets for small Ohnesorge number conditions (e.g., Sallam et al.[9]). The Weber number is proportional to $(U_{air} - U_{liq})^2$ and therefore explains the nonlinear behavior of the jet breakup. As α reduces to low values, the effect of crossflow (aerodynamic forces) rapidly loses significance in the breakup process. This occurs up to the limiting situation of coaxial liquid injection for which larger breakup length would be observed.

Figures 7 and 8 display two series of instantaneous spray images that illustrate the effects of the liquid-to-air momentum flux ratio q on the disintegration process. In Fig. 7 the values of q were changed through variations in U_{air}, maintaining constant the value of V_{liq}. However, in the case described in Fig. 8, the values of q were modified through variations in V_{liq} maintaining constant the value of U_{air}. Fuller et al.[10] observed that, for a given α, the effects of U_{air}

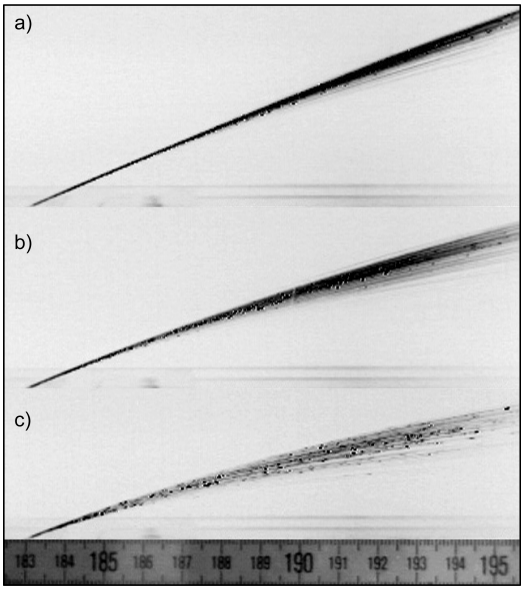

Fig. 7 Instantaneous spray images: effect of the liquid-to-air momentum flux ratio q on the disintegration process: a) test condition 2 (U_{air} = 12.7 m/s and q = 267.3), b) test condition 3 (U_{air} = 27.3 m/s and q = 57.8), and c) test condition 4 (U_{air} = 43.4 m/s and q = 22.9).

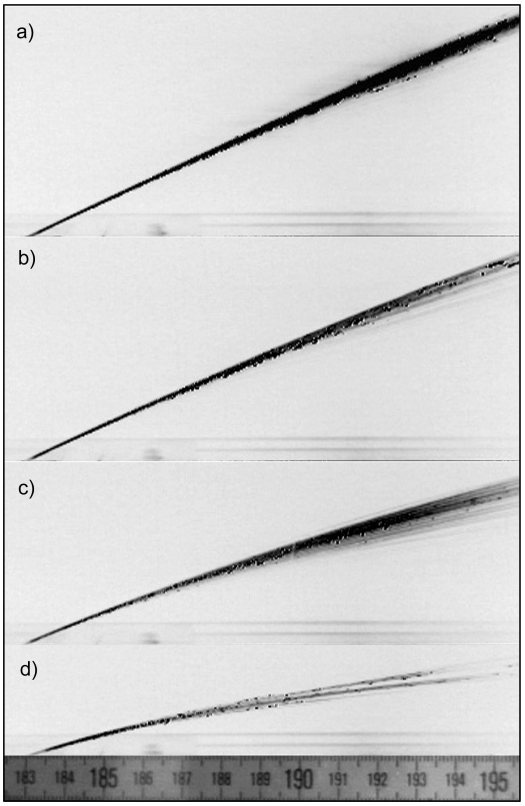

Fig. 8 Instantaneous spray images: effect of the liquid-to-air momentum flux ratio q on the disintegration process: a) test condition 8 (V_{liq} = 23.9 m/s and q = 637.4), b) test condition 7 (V_{liq} = 14.3 m/s and q = 228.2), c) test condition 3 (V_{liq} = 7.2 m/s and q = 57.8), and d) test condition 1 (V_{liq} = 4.8 m/s and q = 25.7).

on jet penetration are insignificant, q being the dominant parameter. In the present work, comparisons among operating conditions with equal injection angle and nearly the same q, for example, comparison between Figs. 7a and 8b, showed that there were also no apparent changes in the overall jet penetration with the increase in V_{liq}. This implies that the noticeable changes in jet penetration that can be seen in Figs. 7 and 8 can be attributed to q alone, although the breakup mechanism cannot, as pointed out by Fuller et al.[10]

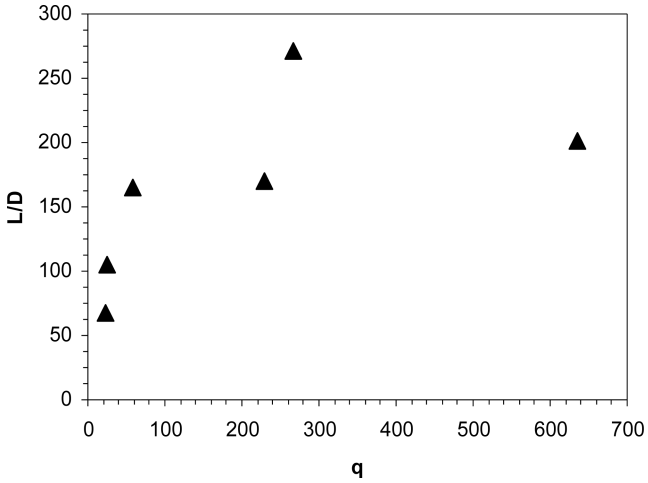

Fig. 9 Effect of the liquid-to-air momentum flux ratio q on the breakup length (test conditions 1, 2, 3, 4, 7, and 8).

In Figs. 7 and 8, q was varied from 22.9 to 267.3 and from 25.7 to 637.4, respectively, which resulted in reductions of the value of u_{rel} from 0.86 to 0.51 in Fig. 7 and from 0.85 to 0.24 in Fig. 8. It can be seen in both figures that as q increases, the liquid jet straightens, the penetration is augmented, and the atomization process deteriorates as a consequence of the reduction in the value of u_{rel}.

Figure 9 shows the variation of the nondimensional breakup length as a function of q for all conditions shown in Figs. 7 and 8. The data in Fig. 9 disclose that initial increases in q significantly diminish the destabilizing aerodynamic forces actuating on the liquid column surface, thereby slowing down the occurrence of jet breakup (see also Figs. 7 and 8). At these relatively low values of U_{air}, the column is disintegrated by liquid turbulence and liquid inertial forces, as can be clearly identified in Figs. 7 and 8, with the effects of the aerodynamic forces being somewhat apparent only at low values of q.

An excellent discussion on breakup regimes of angled liquid injection into subsonic crossflows has been presented by Fuller et al.[10] These authors divided the column breakup process into two distinct regimes: aerodynamic and nonaerodynamic. The dominance of either regime is governed by the jet operating conditions. To predict the breakup regime behavior, based on operating conditions, they defined a breakup regime parameter T_b, as follows:

$$T_b = \frac{3}{2}\frac{V_{liq}}{U_{air} - V_{liq}\cos\alpha}\sqrt{\frac{\rho_{liq}}{\rho_{air}}}We_{liq}^{-\frac{1}{3}} \tag{1}$$

Using this definition, $T_b < 1$ indicates a dominance of aerodynamic forces, whereas $T_b > 1$ indicates a dominance of liquid forces. For the operating conditions used in the present work, Eq. (1) yields values for T_b between 1.8 and 14.8, indicating that the breakup process here is largely governed by the nonaerodynamic mechanism, that is, the breakup is driven by liquid turbulence and liquid initial forces, as discussed earlier.

In the same study, Fuller et al.[10] have also presented empirical correlations to predict breakup lengths for angled liquid injection into subsonic crossflows. These correlations were used to predict the present experimental data of Figs. 6 and 9, but the results showed that they do not satisfactorily predict our data. This is unquestionably because of the different jet operating conditions used in both studies as discussed earlier. An experimental correlation to predict cross-fracture locations y_b in normal liquid injection, has also been proposed by Wu et al.,[4] namely,

$$y_b/D = 3.44q^{\frac{1}{2}} \tag{2}$$

Again, the operating conditions for the just-referenced study differ significantly from those analyzed in the course of this investigation. However, as an attempt to investigate whether the aforementioned

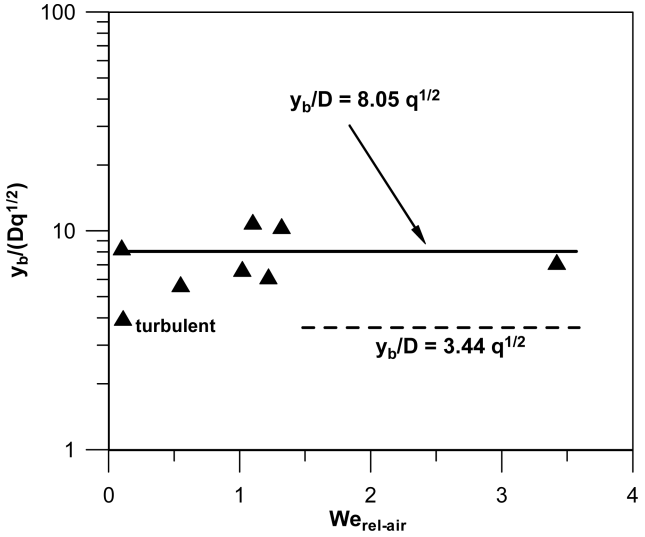

Fig. 10 Effect of the relative air Weber number $We_{rel\text{-}air}$ on the transverse breakup distance (all test conditions).

correlation (or a similar one) might apply to the present data, all investigated conditions have been portrayed in Fig. 10. In this representation, the low range of $We_{rel\text{-}air}$ for our combustor[2] is readily apparent in the abscissa, and the expected dependence of the cross-fracture locations on the square root of q has been properly accounted for in the ordinate. It is clear from Fig. 10 that the limited amount of data available from the present study prevents us to develop a suitable correlation to predict breakup lengths for the jet operating conditions used in this work. Nevertheless, noting that the lower value of $y_b/(Dq^{1/2})$ appearing in Fig. 10 corresponds to a turbulent liquid jet ($Re_{liq} = 3615$), the remaining measurements tend to collapse on the following curve:

$$y_b/D = 8.05q^{\frac{1}{2}} \tag{3}$$

Equation (3), shown as a solid line in Fig. 10, would indicate much higher values of y_b/D for a constant q than those provided by Eq. (2), shown as a dashed line in the same figure. This is not surprising as it might be anticipated that a breakup regime characterized by such low values of $We_{rel\text{-}air}$ would be associated to higher breakup lengths. On the other hand, because of the angled injection, the axial distance to the column fracture point x_b cannot be independent of q as reported by previous authors for normal injection of the liquid. However, as for all investigated conditions, the breakup has occurred before significant bending of the liquid jet by the crossflow takes place; the value of x_b can be simply estimated from the following expression:

$$x_b/D = y_b/D\,\mathrm{cotan}(\alpha) \tag{4}$$

Figures 11–14 show droplet size and velocity (normalized by V_{liq}) distributions along the y direction for test conditions 1, 3, 4, and 5 (see Table 1), respectively. Not surprisingly, in light of the preceding discussion, a glance through these figures reveals that the present jet operating conditions yield Sauter mean diameter (SMD) between around 150 and 350 μm. For conventional combustion applications this is most likely disadvantageous. On the contrary, in the case of our flameless oxidation combustor, which is based on the principle of liquid fuel injection in recirculated hot flue gases,[2] the presence of large droplets might well be beneficial. In fact, smaller droplets are advantageous for fast ignition, as required in conventional premixed or diffusion flames, but, however, are irreconcilable with the concept of flameless oxidation. This is because larger droplets not only delay ignition thus allowing for better mixing between fresh air and recirculated burnt gases prior to their mixing with fuel, but also provide better fuel penetration into the crossflow of the mixed hot gases. Hence, it can be anticipated with reasonable justification that the establishment of flameless oxidation conditions in our

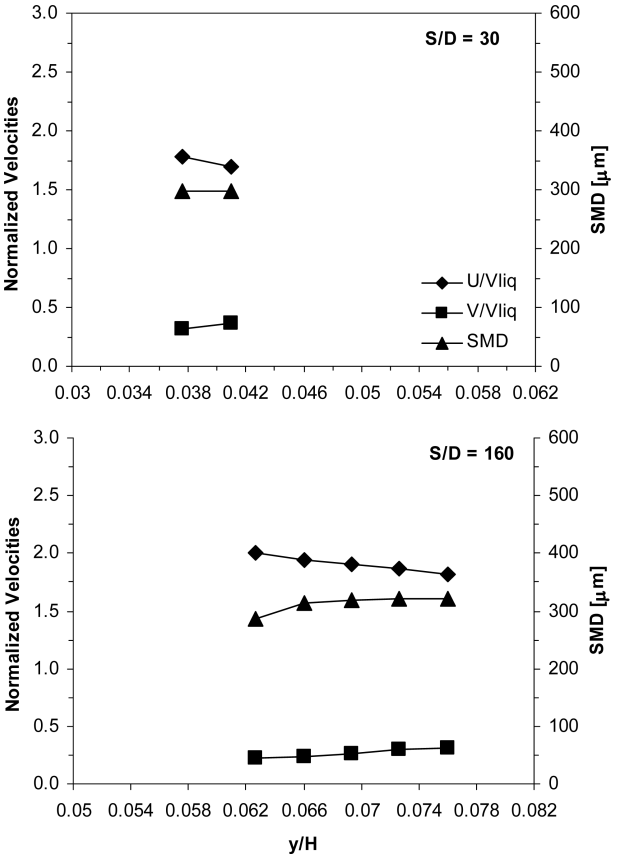

Fig. 11 Droplet size and normalized velocity distributions along the y direction for test condition 1 ($\alpha = 30$ deg, $U_{air} = 27.3$ m/s, $V_{liq} = 4.8$ m/s, and $q = 27.3$) at $S/D = 30$ and 160.

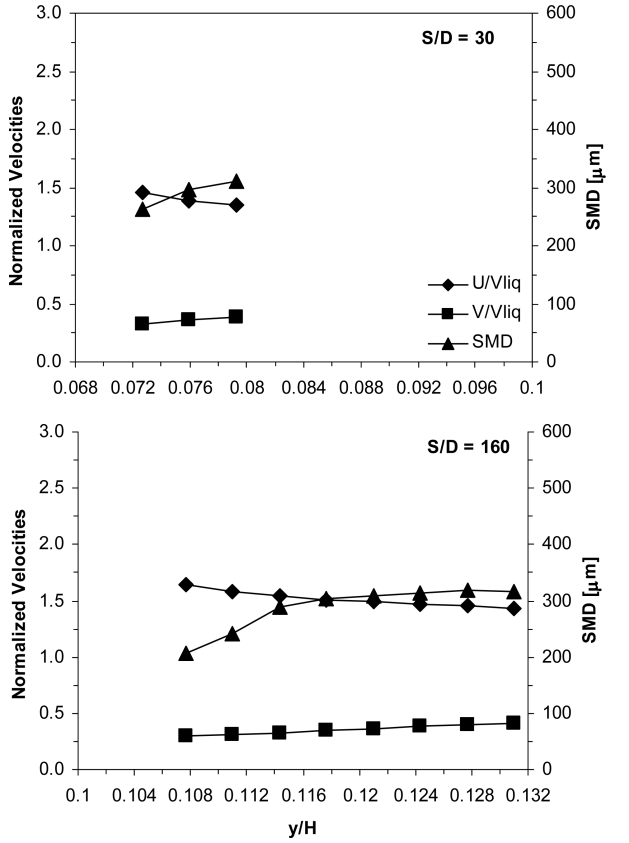

Fig. 12 Droplet size and normalized velocity distributions along the y direction for test condition 3 ($\alpha = 30$ deg, $U_{air} = 27.3$ m/s, $V_{liq} = 7.2$ m/s, and $q = 57.8$) at $S/D = 30$ and 160.

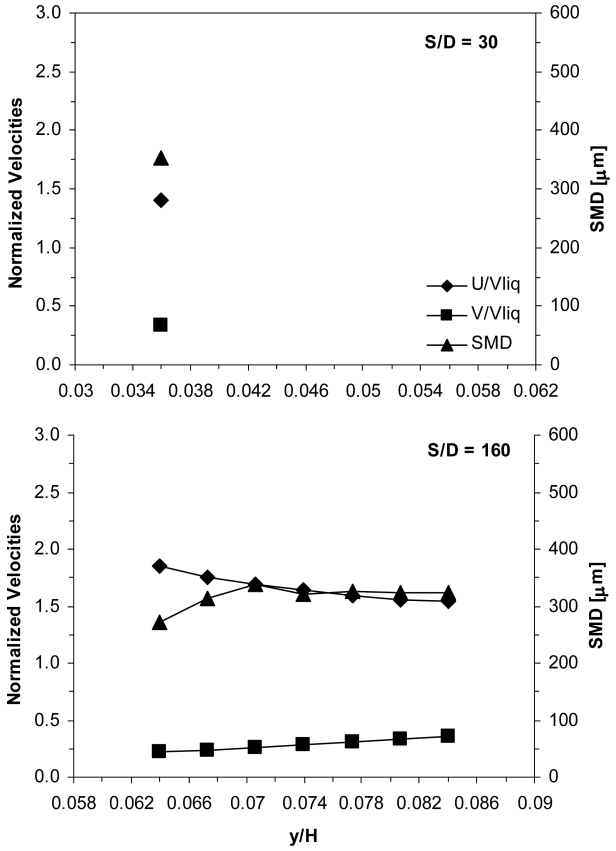

Fig. 13 Droplet size and normalized velocity distributions along the y direction for test condition 4 ($\alpha = 30$ deg, $U_{air} = 43.4$ m/s, $V_{liq} = 7.2$ m/s, and $q = 22.9$) at $S/D = 30$ and 160.

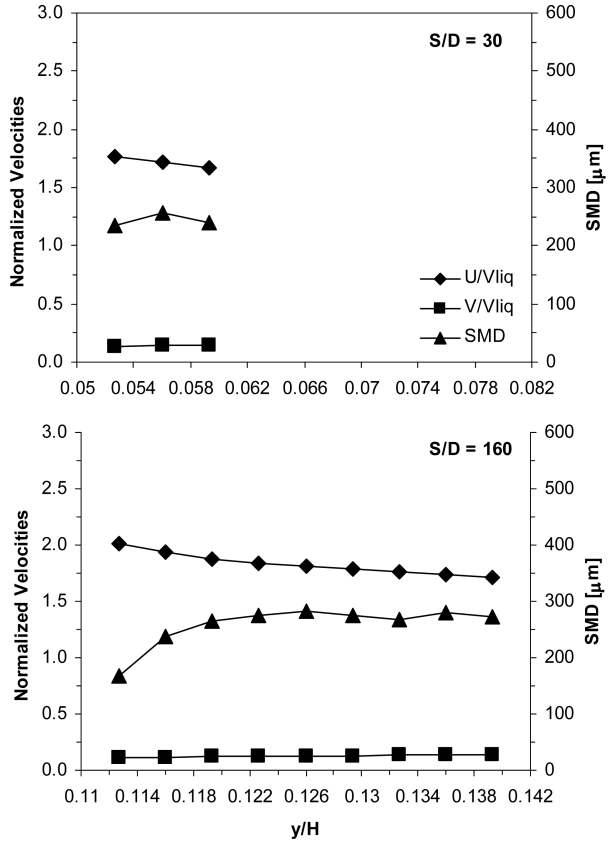

Fig. 14 Droplet size and normalized velocity distributions along the y direction for test condition 5 ($\alpha = 45$ deg, $U_{air} = 27.3$ m/s, $V_{liq} = 7.2$ m/s, and $q = 57.8$) at $S/D = 30$ and 160.

combustor[2] will be most likely achieved in the absence of smaller droplets.

Returning to the discussion of Figs. 11–14, an evident U-velocity/diameter correlation for all droplets is perceptible, with small droplets being faster than larger droplets for all cases presented. Note that all cases studied have in common the fact that U_{air} is always higher than V_{liq}. The observed velocity/size correlation is a rather expected result because the smaller droplets will track the gas phase better as compared with the larger droplets. Another common feature noticeable in Figs. 11–14 is that the droplet U velocities increase significantly with growing air velocity of the crossflow, exhibiting values above the injection liquid velocity because U_{air} is higher than V_{liq} but well below the air velocity. In addition, the crossflow affects the droplet trajectories in such a way that the smaller droplets exhibit lower V velocities as compared with the larger droplets; however, this behavior, according with Sallam et al.,[9] is felt to be an artifact of the relatively fast relaxation times of small droplets compared to large droplets. As for droplet diameters, the sequential panels of Figs. 11–14, at $S/D = 160$, show a gradual increase in the SMD along the y direction, corresponding to a spectrum of droplet sizes produced in the flowing airstream that is skewed vertically. This clearly indicates that the larger droplets penetrate farther into the airstream. It can also be observed in Figs. 11–14 that the values of SMD remain approximately constant when moving downstream from $S/D = 30$ to 160, which suggests that droplet evaporation and coalescence caused by droplet collisions are irrelevant for the jet operating conditions reported herein.

A comparison between Figs. 12 and 14 allows for an evaluation of the influence of the nozzle injection angle on droplet size and normalized velocity distributions along the y direction. At $S/D = 30$ and 160, it is seen that as the value of α increases the SMD values diminish in more than about 50 μm. This behavior is, as discussed earlier, caused by the higher value of u_{rel} associated with the higher injection angle, with the consequent increase of the shear forces actuating on the surface of the liquid jet. Consistently, the droplet U velocities are higher and the droplet V velocities lower for test condition 5.

The analysis of Figs. 11–13 permits the evaluation of the influence of q on droplet size and normalized velocity distributions along the y direction. A comparison between Figs. 11 and 12 allows assessing the influence of q through a modest variation in V_{liq} while maintaining constant U_{air}. Such a comparison reveals that, at $S/D = 30$ and 160, the increase in q affects the droplet mean diameters only at the boundary of the spray near the bottom wall of the wind tunnel yielding smaller droplets. Consequently, larger SMD variations along the y direction are observed during operation with higher value of V_{liq}. This is mainly because of the increased jet instability resulting from the higher liquid jet Reynolds number. As expected, for the conditions with higher value of V_{liq}, the droplet velocities are higher at both measuring locations. The asymmetry in the vertical distribution of droplet size is mainly caused by the influence of the aerodynamic drag force of the droplets. The gradual increase in droplet mean diameters along the y direction corresponds well to the effect of the drag-to-momentum-forces ratio, being larger for the smaller droplets. This phenomenon causes the smaller droplets to follow the host airflow at a faster rate than the larger ones, thus skewing the vertical distribution of droplet size.

A comparison between Figs. 12 and 13 allows for an assessment of the influence of q on the droplet size and normalized velocity distributions along the y direction through a variation in U_{air} while maintaining constant V_{liq}. At $S/D = 30$ the lack of data points in Fig. 13 prevents achieving conclusions; however, at $S/D = 160$, q affects the droplet mean diameters in a manner analogous to that discussed in the preceding paragraph. This reveals again the relevance of q to the droplet mean diameters that result from angled liquid injection. However, in this case the jet with lower q (higher U_{air}) presents, as expected, higher droplet velocities.

Finally, Fig. 15 shows droplet size and velocity (normalized by V_{liq}) distributions along the z direction for test condition 4 (see Table 1). The figure reveals a remarkable uniformity of both droplet size and velocity distributions.

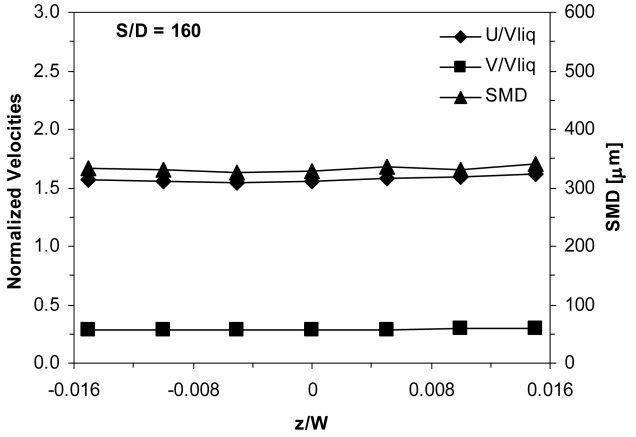

Fig. 15 Droplet size and normalized velocity distributions along the z direction for test condition 4 ($\alpha = 30$ deg, $U_{air} = 43.4$ m/s, $V_{liq} = 7.2$ m/s, and $q = 22.9$) at $S/D = 160$.

Summary

An experimental investigation was performed to study the spray characteristics of liquid jets emerging from angled injection nozzles into subsonic crossflows of air. The experiments were conducted using water as the test liquid and included variations of the nozzle injection angle (15, 30, and 45 deg), air velocity of the crossflow (12.7, 27.3, and 43.4 m/s), and liquid flow rate (4.8, 7.2, 14.3, and 23.9 m/s). The resulting range of dimensionless parameters was as follows: $22.9 \leq q \leq 637.4$; $0.1 \leq We_{rel\text{-}air} \leq 3.42$; $48 \leq We_{liq} \leq 1190.3$; $104 \leq Re_{air} \leq 356$; and $726 \leq Re_{liq} \leq 3615$. An initial assessment of the spray characteristics was performed with the aid of a visualization technique based on video recording and using laser sheet illumination. Following a detailed characterization of the airflow in the tunnel with LDA, detailed droplet size and droplet velocities were obtained for various sprays by the use of PDA. The main findings of this work are as follows:

1) Overall jet penetration and atomization quality are significantly affected by the nozzle injection angle and, to a lesser extent, by the liquid-to-air momentum flux ratio.

2) Breakup length decreases slightly with increasing nozzle injection angle from 15 to 30 deg; however, it decreases significantly with increasing nozzle injection angle from 30 to 45 deg. This suggests that there is a threshold for the aerodynamic forces resulting from the presence of crossflow to effectively disintegrate the liquid column.

3) Breakup length increases with increasing the liquid-to-air momentum flux ratio because the destabilizing aerodynamic forces actuating on the liquid column surface are becoming less significant.

4) There is an evident longitudinal droplet velocity/diameter correlation for all droplets, with small droplets being faster than larger droplets.

5) Droplet longitudinal velocities increase significantly with increasing the crossflow air velocity, exhibiting values above the injection liquid velocity, because U_{air} is higher than V_{liq}, but well below the air velocity.

6) There is a gradual increase in droplet mean diameters along the y direction, which is in accordance with the effect of the drag-to-momentum-forces ratio, being larger in the smaller droplets, thus skewing the spectrum vertically.

7) Droplet mean diameters diminish with increasing the nozzle injection angle as a results of the higher relative air velocity associated with the higher injection angles with the consequent increase of the shear forces actuating on the surface of the liquid jet.

8) Droplet mean diameters are affected only marginally by the liquid-to-air momentum flux ratio, either through changes in air velocity of the crossflow or through the liquid flow rate.

Acknowledgments

Financial support for this work was provided by the European Commission under Contract ENK5-CT 2000-0014 and is acknowledged with gratitude. The second author (M. Melo) is pleased to acknowledge the Fundação para a Ciência e Tecnologia for the provision of a scholarship (SFRH/BD/6345/2001).

References

[1]Wünning, J. A., and Wünning, J. G., "Flameless Oxidation to Reduce Thermal NO-Formation," *Progress in Energy and Combustion Science*, Vol. 23, No. 1, 1997, pp. 81–94.

[2]Levy, Y., Sherbaum, V., and Arfi, P., "Basic Thermodynamics of FLOX-COM, the Low-NO_x Gas Turbines Adiabatic Combustor," *Applied Thermal Engineering*, Vol. 24, Nos. 11–12, 2004, pp. 1593–1605.

[3]Inamura, T., and Nagai, N., "Spray Characteristics of Liquid Jet Traversing Subsonic Airstreams," *Journal of Propulsion and Power*, Vol. 13, No. 2, 1997, pp. 250–256.

[4]Wu, P.-K., Kirkendall, K. A., Fuller, R. P., and Nejad, A. S., "Breakup Processes of Liquid Jets in Subsonic Crossflows," *Journal of Propulsion and Power*, Vol. 13, No. 1, 1997, pp. 64–73.

[5]Wu, P.-K., Kirkendall, K. A., Fuller, R. P., and Nejad, A. S., "Spray Structures of Liquid Jets Atomized in Subsonic Crossflows," *Journal of Propulsion and Power*, Vol. 14, No. 2, 1998, pp. 173–181.

[6]Becker, J., and Hassa, C., "Breakup and Atomization of a Kerosene Jet in Crossflow at Elevated Pressure," *Atomization and Sprays*, Vol. 11, Nos. 1–3, 2002, pp. 49–67.

[7]Rachner, M., Becker, J., Hassa, C., and Doerr, T., "Modelling of the Atomization of a Plain Liquid Fuel Jet in Crossflow at Gas Turbine Conditions," *Aerospace Science and Technology*, Vol. 6, No. 7, 2002, pp. 495–506.

[8]Cavaliere, A., Ragucci, R., and Noviello, C., "Bending and Break-up of a Liquid Jet in a High Pressure Airflow," *Experimental Thermal and Fluid Science*, Vol. 27, No. 4, 2003, pp. 449–454.

[9]Sallam, K. A., Aalburg, C., and Faeth, G. M. "Breakup of Round Nonturbulent Liquid Jets in Gaseous Crossflow," *AIAA Journal*, Vol. 42, No. 12, 2004, pp. 2529–2540.

[10]Fuller, R. P., Wu, P.-K., Kirkendall, K. A., and Nejad, A. S., "Effects of Injection Angle on Atomization of Liquids Jets in Transverse Airflow," *AIAA Journal*, Vol. 38, No. 1, 2000, pp. 64–72.

[11]Tulapurkara, E. G., and Bhalla, V. V. K., "Experimental Investigation of Morel's Method for Wind Tunnel Contractions," *Journal of Fluids Engineering*, Vol. 110, No. 1, 1988, pp. 45–47.

[12]Sousa, J. M. M., and Pereira, J. C. F., "Rollup Region of a Turbulent Trailing Vortex Issued from a Blade with Flow Separation," *Experimental Thermal and Fluid Science*, Vol. 20, Nos. 3–4, 2000, pp. 150–161.

[13]Albrecht, H.-E., Borys, M., Damaschke, N., and Tropea, C., *Laser Doppler and Phase Doppler Measurement Techniques*, Springer-Verlag, Berlin, 2002.

[14]Yanta, W. J., and Smith, R. A. "Measurements of Turbulent-Transport Properties with a Laser Doppler Velocimeter," AIAA Paper 73-169, Jan. 1973.

[15]Erdmann, J. C., and Tropea, C. D., "Turbulence-Induced Statistical Bias in Laser Anemometry," *Proceedings of the Seventh Biennal Symposium on Turbulence*, Sept. 1981.

S. Aggarwal
Associate Editor